4th IASPEI / IAEE International Symposium:

Effects of Surface Geology on Seismic Motion

August 23–26, 2011 · University of California Santa Barbara

ENGINEERING CHARACTERIZATION OF EARTHQUAKE GROUND MOTION COHERENCY AND AMPLITUDE VARIABLITY

Timothy D. Ancheta
PEER
University of California
Berkeley, CA 94720
USA

Jonathan P. Stewart
University of California
Los Angeles, CA 90025
USA

Norman A. Abrahamson
Pacific Gas & Electric Co.
PO Box 770000
San Francisco, CA 94177
USA

ABSTRACT

Earthquake ground motions exhibit spatial variability manifest as random variations of Fourier amplitude and phase. These variations increase with frequency and distance between observations points (ξ), and introduce demands for lifeline systems and foundations. Spatially variable ground motions (SVGM) are quantified by: (1) apparent horizontal wave velocity (V_{app}), which controls wave passage effects that shift Fourier phase; (2) lagged coherency, representing random phase variations; and (3) standard deviation terms representing Fourier amplitude variability. We examine empirical relations for the three SVGM sources through analysis of data from the Borrego Valley Differential Array (BVDA) in California and re-analysis of data from the LSST array in Taiwan, both having a number of stations at $\xi < \sim 120$ m. We show that V_{app} from the two arrays have medians of 2.1 and 2.6 km/s and natural log standard deviations of about 0.5. We show that previous models for lagged coherency and standard deviation from amplitude variability have bias, and propose revisions. We show that amplitude and coherency residuals from the baseline model are uncorrelated, although frequency-to-frequency residuals for both quantities are weakly correlated for small frequency offsets.

INTRODUCTION

Spatial variability of ground motion (SVGM) is an important component in the response of engineered structures such as bridges and buried pipelines (e.g., Der Kiureghian and Neuenhofer, 1991; O'Rourke and Liu, 1999). Assuming homogenous site conditions, SVGM are caused by the wave passage effect and complex source-site wave scattering. As illustrated in Figure 1, wave passage is time delays in wave arrivals due to inclined vertically propagating plane waves or horizontally propagating surface waves. Therefore, the wave passage time delay between two locations introduces a shift in the Fourier phases of earthquake ground motions. Complex waveform scattering occurs as the seismically generated body waves encounter heterogeneities along their source-to-site travel path. Scattering causes random Fourier phase and amplitude variations. Stochastic contributions to phase dominate at high frequencies, and there is a significant level of amplitude variability as well.

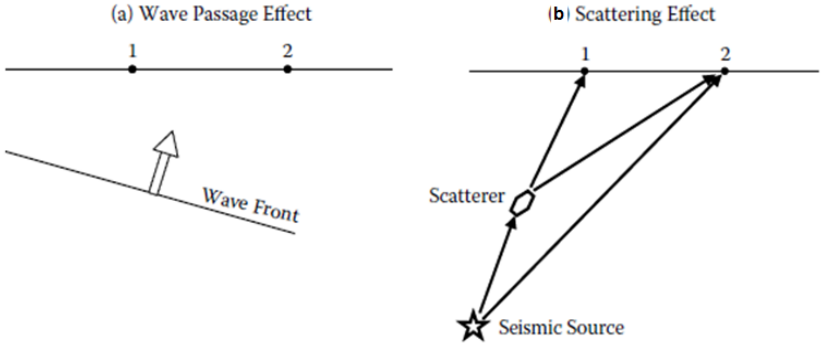

Figure 1. Illustration of wave passage and scattering effects as described by Abrahamson, et al. (1991).Graphic from Zerva (2009).

Ancheta et al. (2011) undertook three phases of work resulting in improved engineering models for characterization of SVGM. The first phase, emphasized in this article, examines fundamental representations of SVGM in the form of phase and amplitude variation models. Additional work presented elsewhere describes the use of those models to simulate spatially variable seismograms from a seed seismogram (Ancheta et al., in review) and predictive models for peak ground strain derived from spatially variable seismograms (Ancheta et al., 2011).

In this article, we use data from the Borrego Valley Differential Array (BVDA), which has not been analyzed previously, to evaluate parameters describing phase and amplitude variability. Coupled with re-analysis of the Lotung, Taiwan array, we use this data to provide recommendations for elements of SVGM that are necessary for waveform simulations.

BORREGO VALLEY DIFFERENTIAL ARRAY AND RECORDED EVENTS

As shown in Figure 2, the Borrego Valley Differential Array (BVDA) is located in an alluvial flood plain that widens to the south. We utilize data from stations 0 (main) and A through E, which are located 10-160 m from the main. The underlying soils consist of medium to very dense, coarse- to medium-grained, sands with S-wave velocities of 400 to 600 m/s. The soil overlies a granitic basement located approximately 230 m below the surface with S-wave velocity of 3 km/s (Kato et al, 1998; Olson et al., 2000). These geologic conditions are similar to the LSST array.

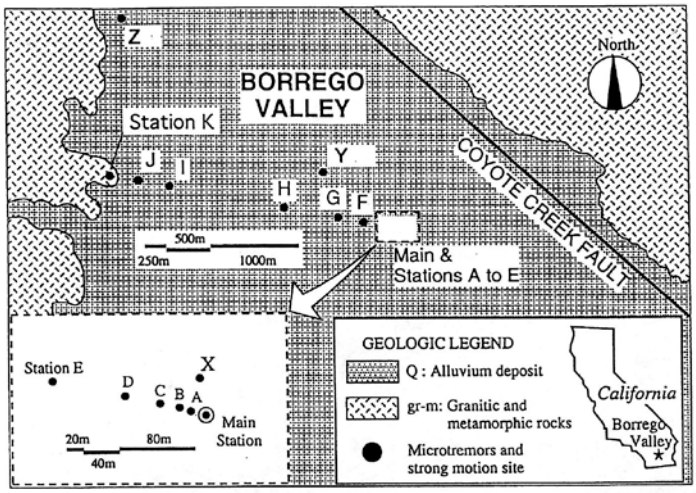

Figure 2. Borrego Valley showing location of BVDA (Kato et al. 1998).

Table 1. Selected earthquake from BVDA

Event No.	Date	Trigger Time	M_L	Epicentral Dist. (km)	Depth (km)	No. of Stations	Window Length (sec)
1	4/9/1995	23:01:31:525	3.3	79.2	8.1	6	5
2	4/11/1995	15:56:52:011	3.4	65.1	9.3	6	5
3	5/7/1995	11:03:44:263	4.8	65.1	10.7	6	10
4	5/7/1995	22:05:45:771	3.0	65.0	9.3	6	5
5	6/9/1995	19:44:11:678	3.4	41.7	14.0	6	5
6	7/28/1995	7:07:41:893	3.6	39.6	8.6	6	10
7	12/25/1995	14:03:40:059	2.6	3.0	11.5	6	5
8	4/6/1997	11:41:27:6	3.1	54.4	11.6	6	2.5
9	5/11/1997	0:16:51:2	3.8	79.4	16.5	6	5
10	5/16/1997	19:36:40:5	2.9	6.5	6.0	6	5
11	5/29/1997	0:48:29:5	3.4	49.4	6.9	5	2.5
12	6/12/1997	15:14:01:00	2.5	12.8	13.9	5	2.5
13	7/26/1997	3:14:59:2	4.9	5.0	13.4	6	5
14	1/2/2002	12:11:22:000	4.2	8.4	12.6	6	5.5
15	9/21/2002	21:26:11:000	4.3	26.2	14.6	4	5
16	10/9/2003	7:33:50:000	3.0	9.8	12.5	4	5

There have been hundreds of earthquakes recorded at BVDA since its installation in 1993. We select earthquakes with recordings having a high signal to noise ratio and minimum 1 sec window length for shear waves to optimize bandwidth. Additionally, we did not select recordings with peak accelerations < 0.005 g. These criteria limit the selected earthquakes to events with M > 2.5, typically with epicentral distances < 80 km.

WAVE PASSAGE AND LAGGED OHERENCY

Definitions

Most theoretical and empirical studies of SVGM have focused on the stochastic and deterministic Fourier phase variability expressed in the form of "lagged coherency" and apparent shear wave propagation velocity, respectively. The mathematical definition of coherency (denoted γ) is given as

$$\gamma_{jk}(f) = \frac{S_{jk}(f)}{\left[S_{jj}(f) S_{kk}(f)\right]^{1/2}} \tag{1}$$

where S_{jj} and S_{kk} are the power spectral density functions of stations j and k, S_{jk} is the cross power spectral density function, and f is frequency. Coherency is a dimensionless complex-valued number that represents variations in Fourier phase between two signals. Perfectly coherent signals have identical phase angles and a coherency of unity. Lagged coherency ($|\gamma|$) is the amplitude of coherency, and represents the contributions of stochastic processes only (no wave passage). Wave passage effects are typically expressed in the

form of an apparent wave propagation velocity. Since coherency measures all sources of phase variation, it is desirable to separate phase variations from different sources using the phasor form of the coherency function:

$$\gamma(\xi, f)_{jk} = \left|\gamma(\xi, f)_{jk}\right| \exp\left[i\theta(\xi, f)_{jk} \right] \tag{2}$$

where the amplitude (lagged coherency) measures phase variations from random effects and the complex phase, θ_{jk}, represents deterministic effects (i.e, wave passage). Both quantify phase difference between two stations *j-k* and are functions of separation distance, ξ, and frequency.

Wave Passage

As shown in Figure 3, wave passage results from delays in arrival times of seismic waves at different locations across a site due to varying site-source distances.

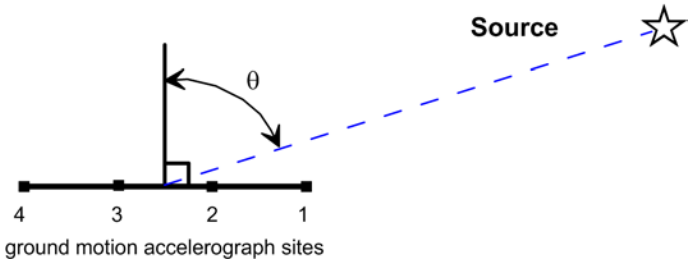

Figure 3.Schematic of station alignment relative to source-site ray path to illustrate wave passage effects.

The critical parameter controlling wave passage is the apparent propagation velocity ($V_{app,\theta}$) of shear waves across the array, which depends on apparent wave speed in the underlying rock (V_{app}) and azimuth angle (θ in Fig. 3) as follows:

$$V_{app,\theta} = \frac{V_{app}}{\sin\theta} \tag{3}$$

The time delay in the wave arrival between two stations can be evaluated from the peak of their cross-correlation. Removing the time lag from one signal aligns the wave arrivals. This method is approximate in the sense that the lag removed from the signals is an average (or aggregate) value over the time window. To minimize this average effect the time lag can be calculated from the S-wave window, which is approximately stationary or from full waveforms when the S-wave window dominates the energy of the record.

Figure 4a shows the peak cross correlation time lag of the radial components of Stations A-E at BVDA relative to a reference station (Main). The ray path for the event is nearly parallel to the array (θ=90 deg). A constant propagation velocity would produce time lags that increase linearly with station separation distance. Figure 4b shows some nonlinearity in this relationship, which is not unusual. Nonetheless, a mean relationship can be derived for a given event, as shown in Fig. 4b, and offsets from the mean are associated with the 'arrival time perturbations' noted previously (Zerva and Zervas, 2002). Alignment of stations on an individual basis for the calculation of lagged coherency removes these arrival time perturbations.

Arrival time perturbations at the Lotung SMART1 array were analyzed by Boissieres and Vanmarcke (1995) using analysis of lags in a manner similar to that described above. Their results indicate a nearly linear increase of lag with distance (similar to Fig. 4b) and significant scatter of the data, which they quantified as a distance-dependent standard deviation term. At distances less than 400 m, this standard deviation in time lag was approximately 2-3 time steps (0.02-0.03 sec). This standard deviation is a quantification of arrival time perturbations. The range of $V_{app,\theta}$ identified was 2.8-6.7 km/s.

The variations of time lag with ξ were evaluated from BVDA data for the events in Table 1 and also for Events 4-7 and 16 recorded at LSST. We use full durations of the recorded signals to compute cross correlation functions for LSST and S-windows for BVDA (due to relatively short durations of LSST data). The inverse of the slope of the trend line ($V_{app,\theta}$), is listed in Table 2. Apparent velocities $V_{app,\theta}$ are relatively scattered (ln standard deviations, σ_{lnV}=0.62-0.84) in comparison to V_{app} (σ_{lnV} =0.54); this indicates that θ has predictive power for wave passage at BVDA and LSST. Accordingly, we use V_{app} and not $V_{app,\theta}$ to represent wave passage, which is consistent with past practice. The values of V_{app} generally range from 1.4-3.8 km/s, with medians of 2.1 km/s for BVDA and 2.6 km/s for LSST. This can be compared to the bedrock shear wave velocity, which ranges from 2.5 to 3 km/sec.

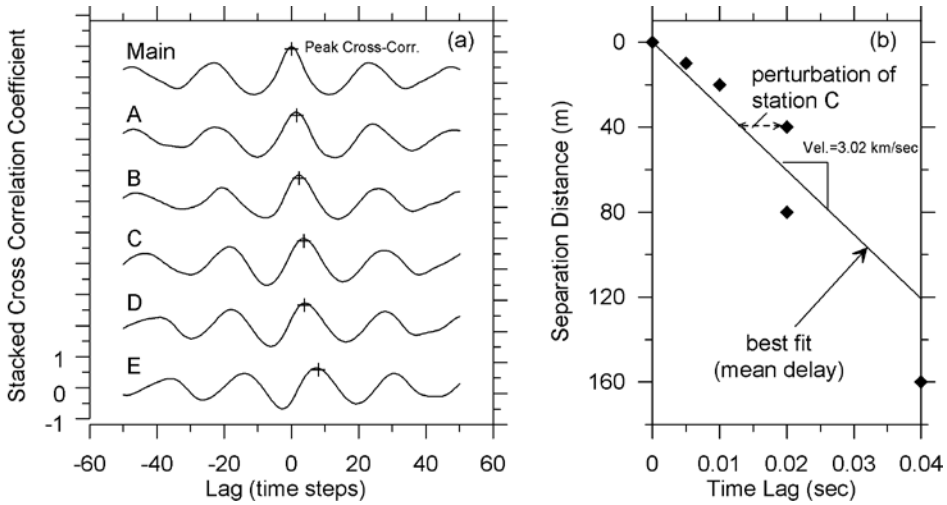

Figure 4. (a) Cross correlation between the reference (Main) and Stations A-E for BVDA Event 8. The plot labeled 'Main' is an autocorrelation. (b) Peak cross correlation time lags across the stations vs. the associated separation distance.

As shown in Figure 5b, residuals of lag times from trend lines show a distance-dependent scatter. At low separation distances (under 80 m), the residuals are below the range of 0.02-0.03 sec found from the SMART 1 data by Boissieres and Vanmarcke (1995). This low level of scatter suggests that arrival time perturbations are likely negligible relative to epistemic uncertainty on V_{app} for this distance range.

Table 2. BVDA and LSST apparent propagation velocities

BVDA Event	θ (deg.)	$V_{app,\theta}$ (m/sec)	V_{app} (m/sec)
2	7	12048	1468
3	7	12270	1495
4	7	11834	1442
5	72	3527	3355
6	63	2959	2636
8	89	3017	3016
9	31	4902	2525
10	2	na	na
11	82	3914	3876
13	2	na	na
14	58	8734	7407
16	31	2999	1544
	σ_{lnV}=	**0.62**	**0.54**
	Med.=	**4408**	**2580**

LSST Event	θ (deg.)	$V_{app,\theta}$ (m/sec)	V_{app} (m/sec)
4	29	11976	5806
5	-69	-2260	2110
6	-84	-1441	1433
7	-105	-2472	2388
16	-84	-1795	1785
	σ_{lnV}=	**0.84**	**0.54**
	Med.=	**2260**	**2110**

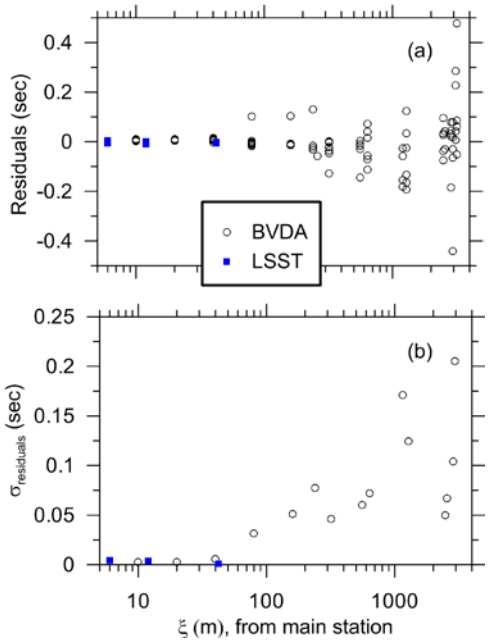

Figure 5. (a) Time lag residuals, (b) standard deviation of residuals versus separation distance

Lagged Coherency

Lagged coherency is the amplitude of the complex-valued coherency function, as indicated in Eq. 2. Physically, it represents the effects of stochastic processes on Fourier phase. To calculate $|\gamma|$, we align each station in an array with the reference station using the cross-correlation approach, which removes arrival time perturbations from the data. To minimize problems with nonstationarity in the data, the S-window is isolated from the remainder of the waveform using windowing procedures (details in Ancheta et al, 2011).

The lagged coherency model of Abrahamson (1992a) is the most commonly used model in practice. It is based on the LSST data, which was processed as described in the previous paragraph. The model presents the inverse hyperbolic tangent of coherency ($\tanh^{-1}|\gamma|$) as a function of frequency and separation distance, ξ, as follows:

$$\tanh^{-1}\left|\gamma\left(f,\xi\right)\right| = a\left(\xi\right)\exp\left\{b\left(\xi\right)f\right\} + k \tag{4}$$

where *a* and *b* are distance-dependent regression parameters. Parameter *k* is fixed at the lagged coherency of noise for the selected level of smoothing, which is calculated as 0.35 (Abrahamson, 1992a).

We used the BVDA data to calculate $\tanh^{-1}|\gamma|$ coherency using the same array processing procedures used to create the LSST model. The data is binned into separation distance ranges of 10, 20, 30-40, 60-70, and 80 m (these are distances between BVDA station pairs). The frequencies at which the coherency is calculated are the center frequencies of the 50% overlapped smoothing windows. At a given frequency, multiple station pairs will contribute data within the distance bin. For the BVDA data set there are two station pairs in each distance bin except for 30-40 m, which has three. Using the two components gives four estimates of $\tanh^{-1}|\gamma|$ coherency. The mean is calculated as the mean of the $\tanh^{-1}|\gamma|$ coherency of the four data points. The resulting mean $\tanh^{-1}|\gamma|$ coherencies calculated from the BVDA selected events are plotted in Figure 6. The LSST mean model is shown along with plus and minus one inter-event standard deviation of 0.26 (ln units). The LSST model fit to the BVDA data is good for $\xi \geq 30$ m for all frequencies, but under-estimates coherency for $\xi = 10$ and 20 m and frequencies < 10 Hz. As shown in Figure 7, similar model misfit at low frequencies and close separation distances has been seen previously in data from the Chiba array whereas the fit to LSST data is good.

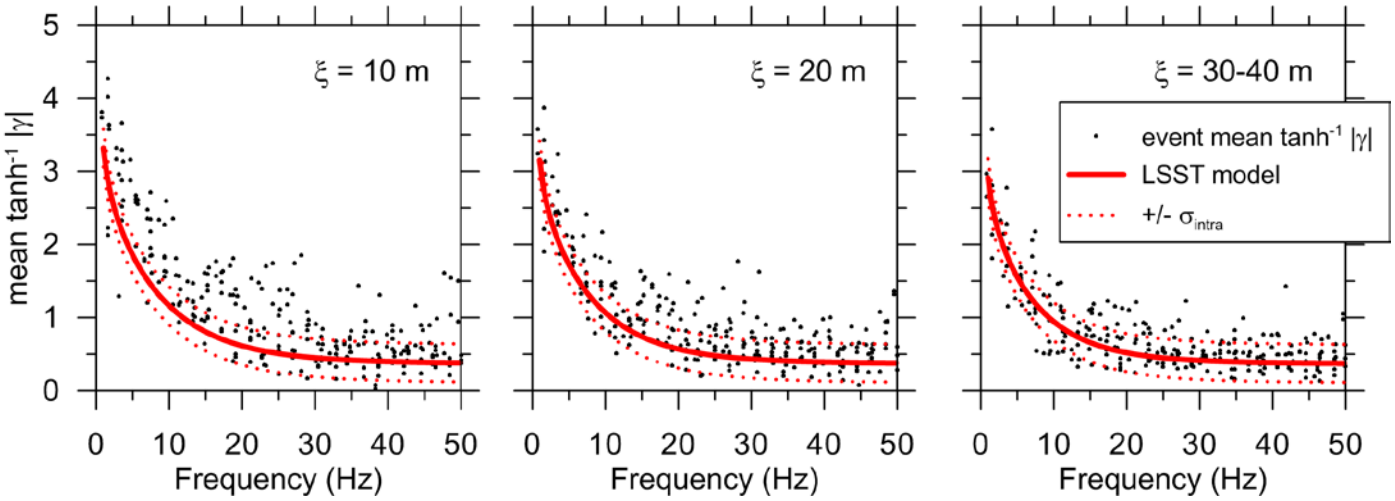

Figure 6.Mean $\tanh^{-1}|\gamma|$ from BVDA data plotted against the LSST model.

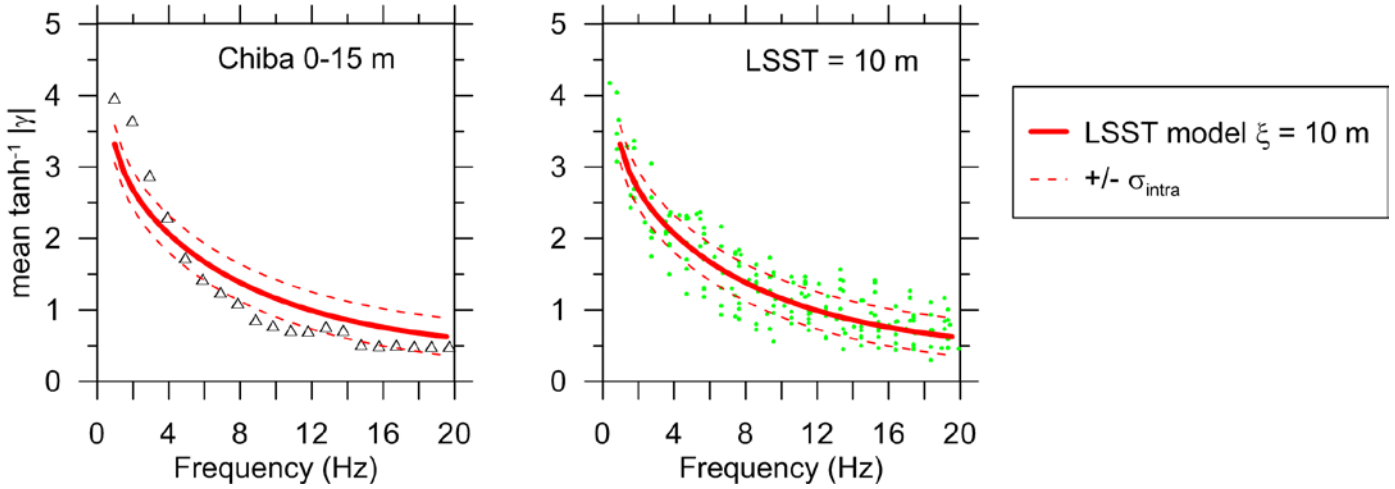

Figure 7.Mean $\tanh^{-1}|\gamma|$ from the Chiba and LSST array plotted against the LSST model. Modified from Abrahamson (2005b).

As described in Ancheta et al. (2011), the aforementioned bias cannot be removed using the regression equation in Eq. 4. To remove the low frequency bias, a second regression is performed with an equation incorporating both exponential and power decay:

$$\tanh^{-1}\left|\gamma\left(f,\xi\right)\right| = a\left(\xi\right)\exp\left\{b\left(\xi\right)f\right\} + d\left(\xi\right)f^{c(\xi)} + k \tag{5}$$

where *a*, *b*, *c*, and *d* are regression parameters while *k* is fixed at 0.35. Since the LSST, BVDA, and Chiba data only support modest modification of the original LSST model of Abrahamson (1992a) at low frequencies and low ξ, we seek only modest adjustments of the regression coefficients. From a parametric study of the model parameters it is apparent that both *a* and *b* affect the position of the coherency function in the range of interest (*a* principally controls coherency at the lower limit of frequency; *b* controls the shape of the curve). Therefore regression is performed with Equation 5 by fixing *c* = -0.878 and *d* = 1/3 (LSST values) and the *a* and *b* parameters are regressed from the BVDA data. The parameters are estimated using least squares regression for each separation distance bin, with the results shown Fig. 8. Figure 8 also compares the nonparametric regression coefficients from the previous section to the coefficients developed by Abrahamson (1992a) from LSST data and to the LSST model, which includes distance-dependence for each parameter.

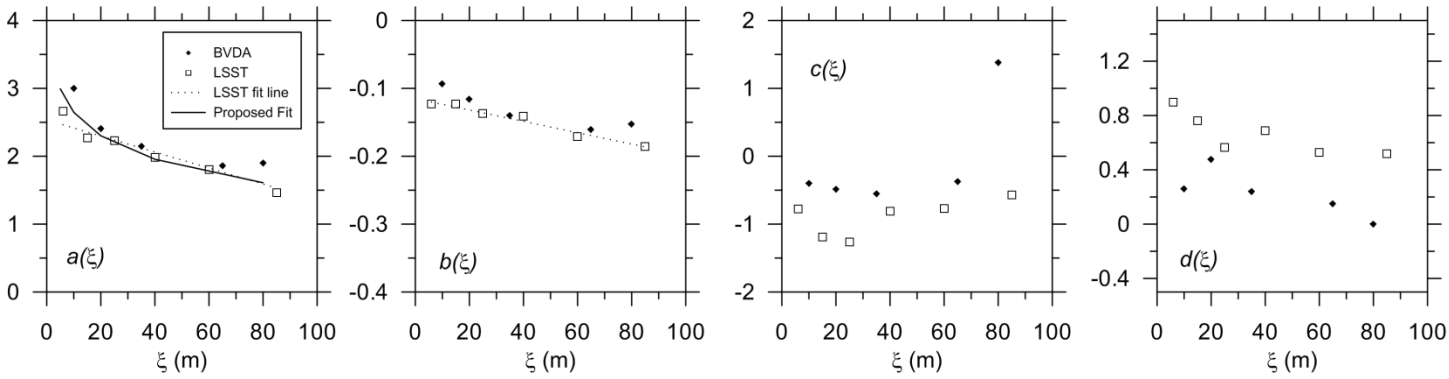

Figure 8. Summary of LSST and BVDA non-parametric estimates of a, b, c, and d for Eq. 5. LSST-based parameters are retained for all coefficients but a.

Including the distance dependence of the coefficients modifies Eq. 5 to:

$$\tanh^{-1}\left|\gamma\left(f,\xi\right)\right| = \left(a_1 + a_2\ln\left(\xi\right)\right)\exp\left\{\left(b_1 + b_2\xi\right)f\right\} + d\left(\xi\right)f^{c(\xi)} + k \tag{6}$$

We perform a simple log-linear regression to fit the *a* regression coefficients from both the BVDA and LSST data (hence, the regression is to re-fit a_1 and a_2). The log-linear function [$a = a_1 + a_2\ln\left(\xi\right)$] was selected because it produces a higher coefficient of determination than a linear fit; the results are shown in Fig. 8. We considered modification of the *b* parameters as well. Values of *b* are higher for BVDA that for LSST, although the slope with distance is approximately the same. We found from comparisons of model predictions to LSST, Chiba, and BVDA data that modification of both the *a* and *b* parameters lead to unacceptable bias relative to the coherency data, specifically poor fit of the Chiba and LSST data. Accordingly, we recommend modification of only the *a* parameters.

Our recommended modification to the LSST model of Abrahamson (1992a) consists of Eq. 6 with all of the original coefficients except for a_1 and a_2, which are modified to a_1= 3.79 and a_2= -0.499. The other coefficients are b_1= -0.115, b_2 = -0.00084, *c* = -0.878, and *d* = 1/3.

The proposed change of the model is checked against the LSST, BVDA, and Chiba array lagged coherency. The proposed new model is plotted with these BVDA and LSST data at ξ = 10 m and 20 m in Figure 9a-b, with the Chiba data for ξ = 5 m in Figure 9c. The low-frequency under-prediction biases in the BVDA and Chiba data sets remain, but are reduced relative to the original LSST model. Some over-prediction bias is introduced relative to the LSST data, which is expected to achieve compromise with the other data sets.

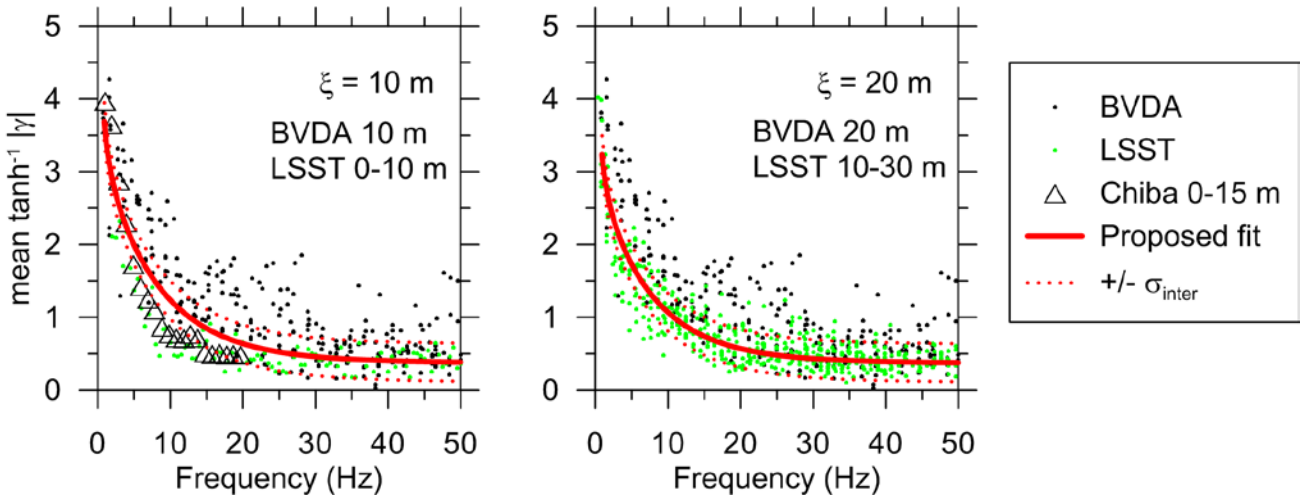

Figure 9.Mean $\tanh^{-1}|\gamma|$ from the BVDA array events for ξ=10 and 20 m compared to adjusted lagged coherency model.

AMPLITUDE VARIABILITY

Studies of dense array recordings (Abrahamson, 1998, 1992a, 2005a, 2005b, Zerva and Zhang, 1996) show that stochastic Fourier amplitude variability contributes to SVGM in addition to the phase variability considered in the previous section. Amplitude variability can be quantified from differences in Fourier amplitudes between recordings at array station pairs. The difference of the natural logs of the amplitudes for a given frequency (f) and station separation (ξ) is denoted $\Delta A(f,\xi)$. If a series of values of ΔA are collected, the distribution should have zero mean assuming the two stations in the pair are close to each other relative to the site-source distance and they have consistent site conditions. The standard deviation of the distribution for $\Delta A(f,\xi)$ is denoted $\sigma_{\Delta A}(f,\xi)$, and is ordinarily calculated assuming intra-event variability dominates relative to inter-event variability (i.e., $\sigma_{\Delta A}$ is assumed to be independent of the event). Note that if σ^2 denotes the variance of an individual recording in the pair, the variance of the difference ($\sigma_{\Delta A}^2$) must be $2\sigma^2$. This is important because only $\sigma_{\Delta A}$ is measureable, and it is used to estimate σ (i.e., $\sigma_{\Delta A} = \sqrt{2}\sigma$).

Since the differential of log Fourier amplitudes is normally distributed with zero mean, an empirical model for the standard deviation, $\sigma_{\Delta A}$, of the amplitude difference can be developed from array data. Using LSST data, an empirical function for $\sigma_{\Delta A}$ using unsmoothed Fourier amplitude spectral ordinates has been developed by Abrahamson (2005b). The model was developed using a maximum likelihood method to compare seven different model forms based on goodness of fit to multiple arrays (details on those arrays are given below). The model form selected by Abrahamson (2005b) is:

$$\sigma_{\Delta A}(f,\xi) = A\left(1 - e^{Bf + Cf\xi}\right) \tag{7}$$

where A, B, and C are the model parameters with values 0.93, 0.163, and –0.0019, respectively. The parameters were selected based on the model fit to the LSST data. The function is applicable for separation distances of 5-100 m and frequencies 0.25-25 Hz.

Abrahamson (2005b) do not plot the model against the LSST data, but we have prepared such a plot as shown in Fig. 10. The model generally compares reasonably well to the data, although there are some regions of bias (over-prediction for f< 10 Hz at ξ=10-20 m; under-prediction for f≈ 15-35 Hz at ξ=30-70 m).

We attempted to regress both LSST data and BVDA data using the functional form in Eq. 7. Differential amplitudes (and standard deviations) are calculated on unsmoothed Fourier amplitudes from the S-window. Convergence of the regression was not achieved, which we found from trial and error to result from poor constraint of the C parameter. Accordingly, we regressed the data from six distance bins for both arrays (LSST and BVDA) using the simpler form below:

$$\sigma_{\Delta A}(f) = A\left(1 - e^{Bf}\right) \tag{8}$$

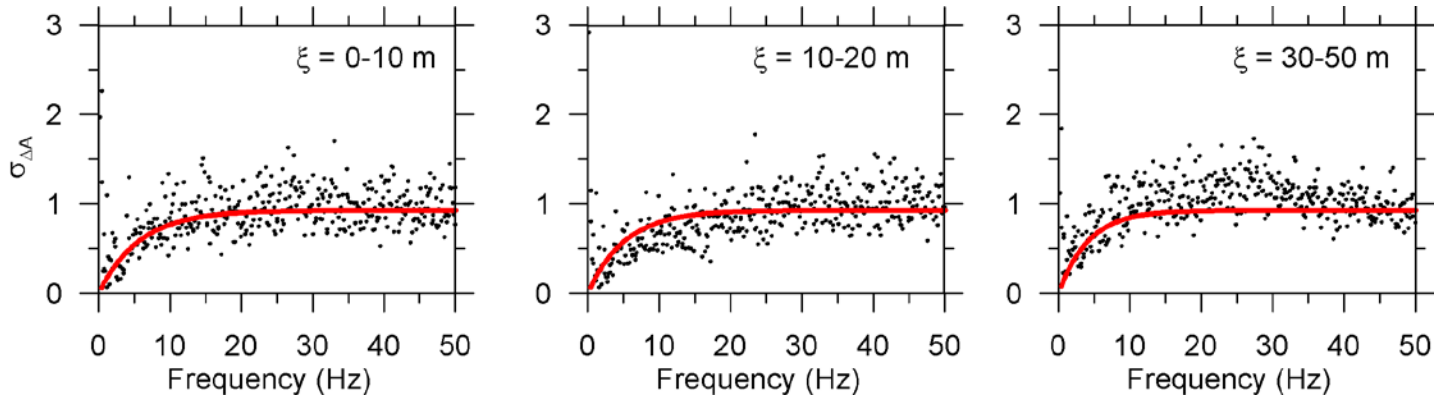

Figure 10.LSST $\sigma_{\Delta A}$ from 9 events considering both horizontal components of motion plotted agains the LSST model.

Values of parameters *A* and *B* are plotted in Figure 11. The results show that *A* is independent of distance whereas *B* varies nearly linearly with distance. Visual inspection of the ordinates shows that *B* can be represented by

$$B = b_1 + b_2 \xi \tag{9}$$

Least-squares linear regression indicates b_1 = -0.1005 (units of 1/m) and b_2 = -0.0025. Figure 12 compares the data from both arrays to the updated model (Eq. 8 with Eq. 9 substituted for *B*). Analysis of the residuals (Ancheta et al., 2011) indicates that the most noticeable misfit are overestimation of $\sigma_{\Delta A}(f)$ in the BVDA data for f< 10 Hz and $\xi \leq 20$ m. This misfit of the BVDA was stronger before the model re-calibration described above. Overall, the adjustment to the model improves the fit to the BVDA data without significantly harming the fit to the LSST data.

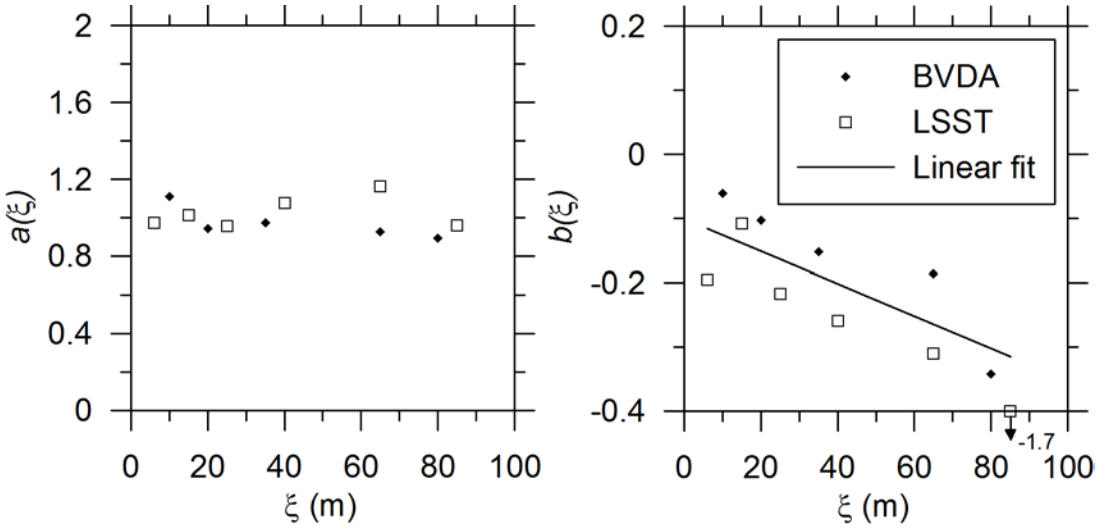

Figure 11. Regression coefficients for $\sigma_{\Delta A}(f)$ model plotted against separation distance

Ancheta et al. (2011) shows that the revised model also provides a good fit to additional soil arrays analyzed previously by Abrahamson (2005b), including Chiba, Hollister differential array, and Imperial Valley differential array. Based on these findings, we recommend that amplitude variability be modeled with the standard deviation model represented by Eqs. 8-9.

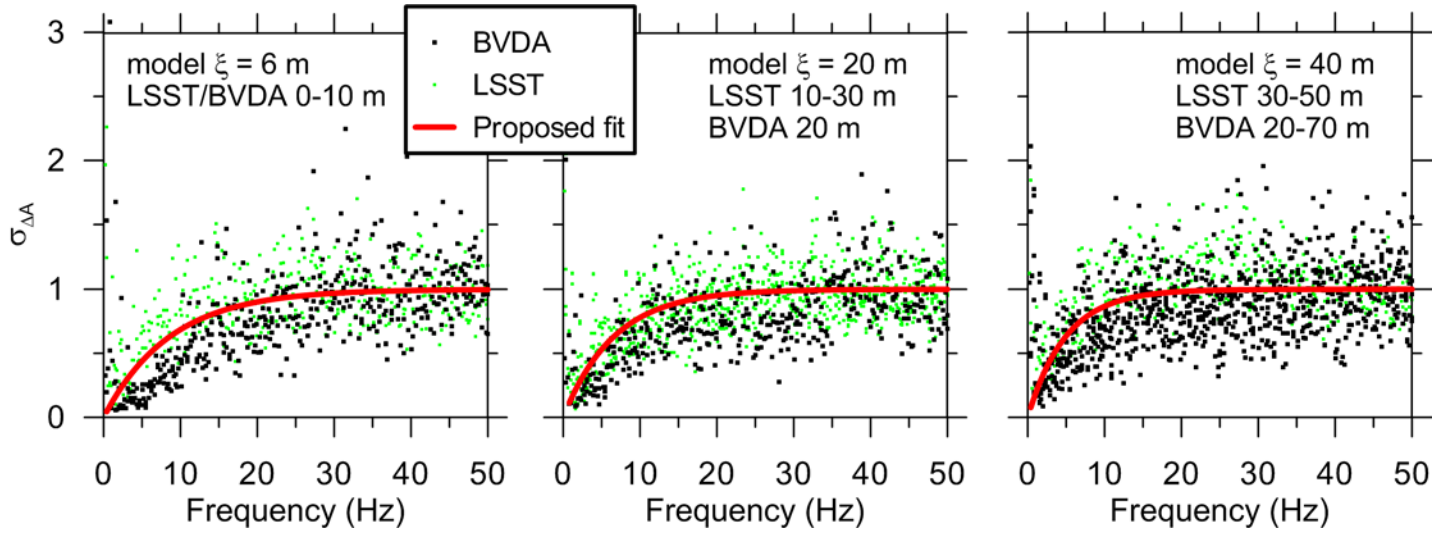

Figure 12. LSST and BVDA sigma and proposed model

CORRELATION COEFFICIENTS

The previous sections have demonstrated the record-to-record variability of phase angle and Fourier amplitude and provided engineering models for this variability. Ground motion simulations utilizing those models should account for any correlations between the various types of variabilities. These issues are investigated in the following sub-sections.

Frequency-To-Frequency Correlation of Coherency and Amplitude Variability

In this section we investigate whether there is a correlation between coherency variability at different frequencies for a given record pair. For example, if the coherency at a given frequency is unusually low with respect to the model given above, does that imply that the coherency would also be low at other frequencies? To examine this issue, we calculate correlation coefficients between residuals derived for different frequencies.

Residuals are calculated as the difference between data and model, which is then normalized by the standard deviation. For lagged coherency, the residual is defined as:

$$R_{\gamma,ij}(f,\xi) = \frac{\tanh^{-1}|\gamma_{ij}| - \tanh^{-1}|\gamma_{m,ij}|}{\sigma_{\gamma}} \tag{10}$$

where $\tanh^{-1}|\gamma_{ij}|$ is the lagged coherency of records i and j at frequency f and separation distance ξ (from data), $\tanh^{-1}|\gamma_{m,ij}|$ is the mean model estimate (calculated using Eq. 6) and $\sigma_{\gamma} = 0.37$. Amplitude residuals are calculated as:

$$R_{\Delta A,ij}(f,\xi) = \frac{\Delta A(f,\xi)}{\sigma_{\Delta A}} \tag{11}$$

where $\sigma_{\Delta A}$ is calculated from Eq. 8 and 9. Eq. 11 assumes that the mean amplitude residual is zero.

The correlation coefficient is calculated as follows for coherency residuals between frequencies f and $f+\Delta f$:

$$\rho_{\gamma}(\Delta f) = \frac{\sum_{k=1}^{p}\left(R_{\gamma,k}(f) - \bar{R}_{\gamma}(f)\right)\times\left(R_{\gamma,k}(f+\Delta f) - \bar{R}_{\gamma}(f+\Delta f)\right)}{\sqrt{\sum_{k=1}^{p}\left(R_{\gamma,k}(f) - \bar{R}_{\gamma}(f)\right)^2 \times \sum_{k=1}^{p}\left(R_{\gamma,k}(f+\Delta f) - \bar{R}_{\gamma}(f+\Delta f)\right)^2}} \tag{12}$$

where k is an index for a given record pair (i.e., records i and j make up a given record pair k), p = number of record pairs, Δf =

frequency step for which the correlation coefficient is calculated and $\overline{R}_{\gamma}(f)$ denotes the average residual for all pairs at frequency f (typically near zero). Note that this manner of computing correlation coefficient does not distinguish between high frequency offsets and low frequency offsets. This extra level of resolution did not appear to be justified by the data.

Correlation coefficients for amplitude variability are calculated as follows for amplitude residuals between frequencies f and $f+\Delta f$:

$$\rho_{\Delta A}(\Delta f) = \frac{\sum_{k=1}^{p}\left(R_{\Delta A,k}(f)-\overline{R}_{\Delta A}(f)\right)\times\left(R_{\Delta A,k}(f+\Delta f)-\overline{R}_{\Delta A}(f+\Delta f)\right)}{\sqrt{\sum_{k=1}^{p}\left(R_{\Delta A,k}(f)-\overline{R}_{\Delta A}(f)\right)^2\times\sum_{k=1}^{p}\left(R_{\Delta A,k}(f+\Delta f)-\overline{R}_{\Delta A}(f+\Delta f)\right)^2}} \quad (13)$$

where $\overline{R}_{\Delta A}(f)$ denotes the average residual for all pairs at frequency f (typically near zero) and all other terms are as defined above.

Figure 13a plots coherency correlation coefficients against frequency step (Δf). The red lines indicate the running median and are intended to show the data trend. As shown in the figure, there is a non-zero correlation between coherency residuals for frequency steps below about 2-3 Hz, but the correlations are weak. Figure 13b shows amplitude correlation coefficients calculated using Eq. 13. The correlation decreases according to a nearly log-linear trend from about 0.2 at Δf =0.4 Hz to effectively 0 for Δf>10 Hz.

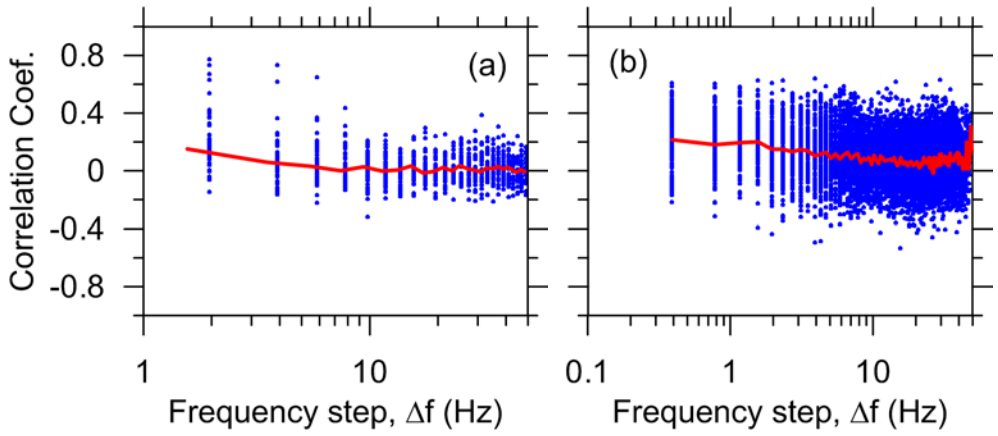

Figure 13. Correlation coefficient between frequencies for residuals of coherency (a) and amplitude variability (b) measured from BVDA Events 1, 2, 3, 6, and 8. These events have common S-window durations, causing sampled frequencies to be aligned.

Correlation of Amplitude Variability and Coherency

In the previous section, we have shown that frequency-to-frequency variations of phase and amplitude variability are weakly correlated. In this section we investigate the extent to which coherency and amplitude variability at the same frequency are correlated.

Previous investigators have commented on possible relationships between amplitude variability and coherency. For example, Abrahamson (1992a) observed that peaks and troughs in the Fourier amplitude spectrum seem to be associated with peaks and troughs in coherency residuals. However, any possible correlation was neglected in the time history simulation procedure of Abrahamson (1992b). The work of Zerva and Zhang (1997) and Zerva and Zervas (2002) established envelope functions for amplitude and phase variability that follow similar trends. In particular, the envelope functions demonstrate similar increases with frequency, both approaching their maximum values at about 9 Hz. Zerva and Zervas (2002) postulate that the same physical processes causing phase variability also contribute to amplitude variability. In particular, they describe how at low frequencies the wavelengths are long and are unaffected by local variations in soil/rock media, whereas at higher frequencies the random variations increase as the contributions of scattered waves and site response variability increase. It should be noted, however, that this correlation described by Zerva and co-authors concerns the envelop functions themselves. No comment is made on correlation attributes of the amplitude and phase variability of individual record sets. We investigate this possibility below.

In particular we investigate the correlation of normalized residuals of data relative to the coherency and amplitude variability models. The normalized residuals are calculated using Eq. 10 and 11. These calculations are performed using the BVDA data set for frequency ranges 0-5 Hz, 5-10 Hz, 10-15 Hz, and 15-20 Hz and separation distances ξ = 10 and 20 m. Figure 14 shows that the correlation coefficients are nearly zero.

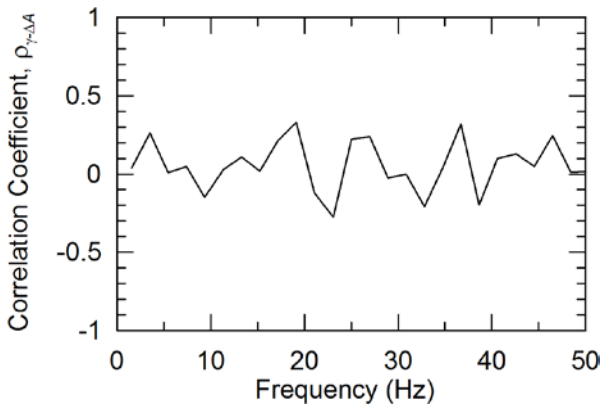

Figure 14. Correlation coefficients between amplitude and coherency residuals for separation distances ξ = 10 and 20 m.

CONCLUSIONS AND RECOMMENDATIONS

Spatially variable ground motions (SVGMs) are defined as the difference in the earthquake ground motions at two relatively nearby locations having similar site conditions. This variability can be represented by differences in Fourier phase and amplitude. A number of physical processes give rise to SVGMs. Wave passage causes delays in wave arrivals at different locations across a site due to slightly different path lengths relative the source. Independent of wave passage, the stochastic differences in the Fourier amplitude and phase are caused by complex wave scattering. The stochastic phase variation can be described by lagged coherency functions, while stochastic amplitude variability is characterized by standard deviation terms that represent dispersion around a mean amplitude.

The SVGM components of random phase variability due to complex wave scattering (e.g. lagged coherency) and phase delay related to the wave passage effect have been investigated previously. Other significant components of SVGM have only been examined in inaccessible literature and in some cases their evaluation is incomplete. These parameters include standard deviation terms describing Fourier amplitude variability ($\sigma_{\Delta A}$), and correlation coefficients between lagged coherency and Fourier amplitude variability. Therefore, current SVGM simulation routines have incorporated a limited set of the total causes of SVGM, namely phase variability due to wave scattering and wave passage due to an inclined body wave.

In this paper we investigate SVGM parameters applicable to short separation distances (< ~100 m) while focusing on metrics not well documented in the literature. This work is part of broader research program and supports the development of a simulation routine than can incorporate all unique contributing sources of SVGM simultaneously. That routine, in turn, has been used to estimate the effect of SVGM on extension ground strains in large ground motions (Ancheta et al., 2011).

Examination of wave passage from the BVDA and LSST data indicates that plane wave propagation characterized by an apparent propagation velocity V_{app} explains most of the time lags between stations evaluated from cross-correlation. Additional variability, known as arrival time perturbations, is practically negligible relative to epistemic uncertainty on V_{app} for short separation distances (< 100 m). The median V_{app} from the BVDA and LSST data was 2.6 and 2.1 km/s, respectively, both having a ln standard deviation of σ_{lnV}=0.5. These values are within the typical range of 2-3.5 km/sec measured at other arrays.

Comparison of the lagged coherency and $\sigma_{\Delta A}$ from the BVDA data confirms that the LSST model over-predicts both at low frequencies for $\xi \leq$ 20 and 60 m, respectively. A proposed model correction through the use of a combined LSST/BVDA data regression removed some of the observed bias.

We find that lagged coherency and Fourier amplitude variability model residuals are uncorrelated. This means that a simulation routine that uses these SVGM parameters in a forward sense must use independent random variables for both the stochastic Fourier amplitude and phase. A correlation study on the frequency-to-frequency Fourier amplitude and coherency difference between array station pairs shows they are weakly correlated. The correlation was shown to decrease along a log-linear trend from about 0.2 at Δf =

0.4 Hz to effectively 0 for Δf >10 Hz for Fourier amplitude differences and > 3 Hz for Fourier phase differences. Due to the weak correlations, the simulation routine incorporating stochastic variability should use independent random variables at each frequency.

ACKNOWLEDGEMENTS

Support for this study was provided by a grant from California Earthquake Authority administered through the Consortium of Universities for Research in Earthquake Engineering and the Dissertation Year Fellowship from UCLA. This support is gratefully acknowledged. Drs. Jamie Steidl of UCSB and Robert Nigbor of UCLA are thanked for providing access to the BVDA data. Norman Abrahamson is thanked for his helpful comments on this topic.

REFERENCES

Abrahamson, N.A., J.F. Schneider, and J.C. Stepp [1991], "Empirical Spatial Coherency Functions for Applications to Soil-Structure Interaction Analyses," Earthquake Spectra. Vol. 7, No. 1, pp. 1-27.

Abrahamson, N.A. [1992a], "Spatial Variation of Earthquake Ground Motion for Application to Soil-Structure Interaction," Electrical Power Research Institute, Rpt. No. EPRI TR-100463

Abrahamson, N.A. [1992b], "Generation of Spatially Incoherent Strong Motion Time Histories," Proc. 10th World Conf. Earthquake Eng., 845-850.

Abrahamson, N.A. [2005a], "Spatial Coherency Models for Soil-Structure Interaction," (Unpublished).

Abrahamson, N.A. [2005b], "Effect of Local Site Condition on Spatial Coherency," Electric Power Research Institute, Rpt. No.RP2978-05.

Ancheta, T.D., J.P. Stewart, and N.A. Abrahamson [2011], "Engineering Characterization of Spatially Variable Earthquake Ground Motions," *Report No. PEER-2011/xx*, Pacific Earthquake Engineering Research Center, in preparation.

Boissieres, H.-P. and E.H. Vanmarcke [1995], "Estimation of Lags for a Seismograph Array: Wave Propagation and Composite Correlation," Soil Dynamics and Earthquake Engineering, Vol. 14, No. 1, pp 5-22.

Der Kiureghian A and Neuenhofer A (1992), Response spectrum method for multiple support seismic excitation, *Earthquake Eng. Struct. Dyn.* Vol. 21, No. 8, pp 713–740.

Kato, K., T. Takemura, S. Uchiyama, S. Iizuka, and R.L. Nigbor [1998], "Borrego Valley Downhole Array in Southern California: Instrumentation and Preliminary site effect study," Proc. 2nd Int. Sym. on the Effects of Surface Geology on Seismic Motion, Yokohama, Japan.

O'Rourke, M.J. and X. Liu [1999]. "Response of Buried Pipelines Subject to Earthquake Effects" Multidisciplinary Center for Earthquake Engineering Research, University of Buffalo, NY. ISBN 0-9656682-3-1.

Olson, K.B., R.L. Nigbor, and T. Konno [2000], "3D Viscoelastic Wave Propagation in the Upper Borrego Valley, California, Constrained by Borehole and Surface Data," Bull. Seism. Soc. Am., Vol. 90, No. 1, pp. 134-150.

Zerva, A. [2009], "*Spatial Variation of Seismic Ground Motions*," CRC Press, Taylor and Francis Group, Florida.

Zerva, A. and V. Zervas [2002], "Spatial Variation of Seismic Ground Motions: An Overview," Appl Mech Rev, Vol. 55, No. 3, pp. 271-297.

Zerva, A. and O. Zhang [1996], "Estimation of Signal Characteristics in Seismic Ground Motions," Probabilistic Engineering Mechanics, Vol. 11, No. 4, pp. 229-242.

Zerva, A. and O. Zhang [1997], "Correlation Patterns in Characteristics of Spatially Variable Seismic Ground Motions," Earthquake Engineering and Structural Dynamics, Vol. 26, No. 1, pp. 19-39.